ELSEVIER

Nuclear Physics A698 (2002) 64c–77c

NUCLEAR PHYSICS A

www.elsevier.com/locate/npe

Results from the STAR Experiment

John W. Harris[a] for the STAR Collaboration

[a]Physics Department, Yale University
P.O. Box 208124, New Haven, CT 06520-8124 U.S.A.

C. Adler[11], Z. Ahammed[23], C. Allgower[12], J. Amonett[14], B.D. Anderson[14], M. Anderson[5], G.S. Averichev[9], J. Balewski[12], O. Barannikova[9,23], L.S. Barnby[14], J. Baudot[13], S. Bekele[20], V.V. Belaga[9], R. Bellwied[30], J. Berger[11], H. Bichsel[29], L.C. Bland[12], C.O. Blyth[3], B.E. Bonner[24], R. Bossingham[15], A. Boucham[26], A. Brandin[18], H. Caines[20], M. Calderón de la Barca Sánchez[31], A. Cardenas[23], J. Carroll[15], J. Castillo[26], M. Castro[30], D. Cebra[5], S. Chattopadhyay[30], M.L. Chen[2], Y. Chen[6], S.P. Chernenko[9], M. Cherney[8], A. Chikanian[31], B. Choi[27], W. Christie[2], J.P. Coffin[13], L. Conin[26], T.M. Cormier[30], J.G. Cramer[29], H.J. Crawford[4], M. DeMello[24], W.S. Deng[14], A.A. Derevschikov[22], L. Didenko[2], J.E. Draper[5], V.B. Dunin[9], J.C. Dunlop[31], V. Eckardt[16], L.G. Efimov[9], V. Emelianov[18], J. Engelage[4], G. Eppley[24], B. Erazmus[26], P. Fachini[25], E. Finch[31], Y. Fisyak[2], D. Flierl[11], K.J. Foley[2], J. Fu[15], N. Gagunashvili[9], J. Gans[31], L. Gaudichet[26], M. Germain[13], F. Geurts[24], V. Ghazikhanian[6], J. Grabski[28], O. Grachov[30], D. Greiner[15], V. Grigoriev[18], M. Guedon[13], E. Gushin[18], T.J. Hallman[2], D. Hardtke[15], J.W. Harris[31], M. Heffner[5], S. Heppelmann[21], T. Herston[23], B. Hippolyte[13], A. Hirsch[23], E. Hjort[15], G.W. Hoffmann[27], M. Horsley[31], H.Z. Huang[6], T.J. Humanic[20], H. Hümmler[16], G. Igo[6], A. Ishihara[27], Yu.I. Ivanshin[10], P. Jacobs[15], W.W. Jacobs[12], M. Janik[28], I. Johnson[15], P.G. Jones[3], E. Judd[4], M. Kaneta[15], M. Kaplan[7], D. Keane[14], A. Kisiel[28], J. Klay[5], S.R. Klein[15], A. Klyachko[12], A.S. Konstantinov[22], L. Kotchenda[18], A.D. Kovalenko[9], M. Kramer[19], P. Kravtsov[18], K. Krueger[1], C. Kuhn[13], A.I. Kulikov[9], G.J. Kunde[31], C.L. Kunz[7], R.Kh. Kutuev[10], A.A. Kuznetsov[9], L. Lakehal-Ayat[26], J. Lamas-Valverde[24], M.A.C. Lamont[3], J.M. Landgraf[2], S. Lange[11], C.P. Lansdell[27], B. Lasiuk[31], F. Laue[2], A. Lebedev[2], T. LeCompte[1], V.M. Leontiev[22], P. Leszczynski[28], M.J. LeVine[2], Q. Li[30], Q. Li[15], S.J. Lindenbaum[19], M.A. Lisa[20], T. Ljubicic[2], W.J. Llope[24], G. LoCurto[16], H. Long[6], R.S. Longacre[2], M. Lopez-Noriega[20], W.A. Love[2], D. Lynn[2], R. Majka[31], A. Maliszewski[28], S. Margetis[14], L. Martin[26], J. Marx[15], H.S. Matis[15], Yu.A. Matulenko[22], T.S. McShane[8], F. Meissner[15], Yu. Melnick[22], A. Meschanin[22], M.L. Miller[31], Z. Milosevich[7], N.G. Minaev[22], J. Mitchell[24], V.A. Moiseenko[10], D. Moltz[15], C.F. Moore[27], V. Morozov[15], M.M. de Moura[30], M.G. Munhoz[25], G.S. Mutchler[24], J.M. Nelson[3], P. Nevski[2], V.A. Nikitin[10], L.V. Nogach[22], B. Norman[14], S.B. Nurushev[22], J. Nystrand[15], G. Odyniec[15], A. Ogawa[21], V. Okorokov[18], M. Oldenburg[16], D. Olson[15], G. Paic[20], S.U. Pandey[30], Y. Panebratsev[9], S.Y. Panitkin[14], A.I. Pavlinov[30], T. Pawlak[28], V. Perevoztchikov[2], W. Peryt[28], V.A Petrov[10], W. Pinganaud[26], E. Platner[24], J. Pluta[28], N. Porile[23], J. Porter[2], A.M. Poskanzer[15],

0375-9474/02/$ – see front matter
PII S0375-9474(01)01349-5

E. Potrebenikova[9], D. Prindle[29],C. Pruneau[30], S. Radomski[28], G. Rai[15], O. Ravel[26], R.L. Ray[27], S.V. Razin[9,12], D. Reichhold[8], J.G. Reid[29], F. Retiere[15], A. Ridiger[18], H.G. Ritter[15], J.B. Roberts[24], O.V. Rogachevski[9], J.L. Romero[5], C. Roy[26], D. Russ[7], V. Rykov[30], I. Sakrejda[15], J. Sandweiss[31], A.C. Saulys[2], I. Savin[10], J. Schambach[27], R.P. Scharenberg[23], K. Schweda[15], N. Schmitz[16], L.S. Schroeder[15], A. Schüttauf[16], J. Seger[8], D. Seliverstov[18], P. Seyboth[16], K.E. Shestermanov[22], S.S. Shimanskii[9], V.S. Shvetcov[10], G. Skoro[9], N. Smirnov[31], R. Snellings[15], J. Sowinski[12], H.M. Spinka[1], B. Srivastava[23], E.J. Stephenson[12], R. Stock[11], A. Stolpovsky[30], M. Strikhanov[18], B. Stringfellow[23], H. Stroebele[11], C. Struck[11], A.A.P. Suaide[30], E. Sugarbaker[20], C. Suire[13], T.J.M. Symons[15], A. Szanto de Toledo[25], P. Szarwas[28], J. Takahashi[25], A.H. Tang[14], J.H. Thomas[15], V. Tikhomirov[18], T.A. Trainor[29], S. Trentalange[6], M. Tokarev[9], M.B. Tonjes[17], V. Trofimov[18], O. Tsai[6], K. Turner[2], T. Ullrich[2], D.G. Underwood[1], G. Van Buren[2], A.M. VanderMolen[17], A. Vanyashin[15], I.M. Vasilevski[10], A.N. Vasiliev[22], S.E. Vigdor[12], S.A. Voloshin[30], F. Wang[23], H. Ward[27], J.W. Watson[14], R. Wells[20], T. Wenaus[2], G.D. Westfall[17], C. Whitten Jr. [6], H. Wieman[15], R. Willson[20], S.W. Wissink[12], R. Witt[14], N. Xu[15], Z. Xu[31], A.E. Yakutin[22], E. Yamamoto[6], J. Yang[6], P. Yepes[24], A. Yokosawa[1], V.I. Yurevich[9], Y.V. Zanevski[9], J. Zhang[15], W.M. Zhang[14], R. Zoulkarneev[10], A.N. Zubarev[9]

[1]Argonne National Laboratory, Argonne, Illinois 60439 [2]Brookhaven National Laboratory, Upton, New York 11973 [3]University of Birmingham, Birmingham, United Kingdom [4]University of California, Berkeley, California 94720 [5]University of California, Davis, California 95616 [6]University of California, Los Angeles, California 90095 [7]Carnegie Mellon University, Pittsburgh, Pennsylvania 15213 [8]Creighton University, Omaha, Nebraska 68178 [9]Laboratory for High Energy (JINR), Dubna, Russia [10]Particle Physics Laboratory (JINR), Dubna, Russia [11]University of Frankfurt, Frankfurt, Germany [12]Indiana University, Bloomington, Indiana 47408 [13]Institut de Recherches Subatomiques, Strasbourg, France [14]Kent State University, Kent, Ohio 44242 [15]Lawrence Berkeley National Laboratory, Berkeley, California 94720 [16]Max-Planck-Institut fuer Physik, Munich, Germany [17]Michigan State University, East Lansing, Michigan 48824 [18]Moscow Engineering Physics Institute, Moscow Russia [19]City College of New York, New York City, New York 10031 [20]Ohio State University, Columbus, Ohio 43210 [21]Pennsylvania State University, University Park, Pennsylvania 16802 [22]Institute of High Energy Physics, Protvino, Russia [23]Purdue University, West Lafayette, Indiana 47907 [24]Rice University, Houston, Texas 77251 [25]Universidade de Sao Paulo, Sao Paulo, Brazil [26]SUBATECH, Nantes, France [27]University of Texas, Austin, Texas 78712 [28]Warsaw University of Technology, Warsaw, Poland [29]University of Washington, Seattle, Washington 98195 [30]Wayne State University, Detroit, Michigan 48201 [31]Yale University, New Haven, Connecticut 06520

1. Introduction

Collisions of heavy ions at RHIC are expected to exceed the energy densities required to achieve a phase transition to the quark gluon plasma (QGP) [1,2]. STAR was designed and constructed to investigate the behavior of strongly interacting matter at high energy density and to search for signatures of QGP formation and chiral symmetry restoration in

collisions at RHIC [3]. Initially STAR will focus on measurements of hadron production and the study of global observables. The STAR physics program also includes: the measurement of products from ultra-peripheral heavy ion collisions to study photon and pomeron interactions [4]; proton-proton interactions and proton-nucleus interactions to understand nuclear parton distribution functions and for heavy ion reference data; and a complete program of spin physics utilizing collisions of polarized protons at RHIC to measure the contribution of the spin of the gluon and of sea-quarks to the spin structure function of the proton [5]. In this paper, we report results for collisions of Au + Au at $\sqrt{s_{NN}} = 130$ GeV from the STAR experiment in the first RHIC run.

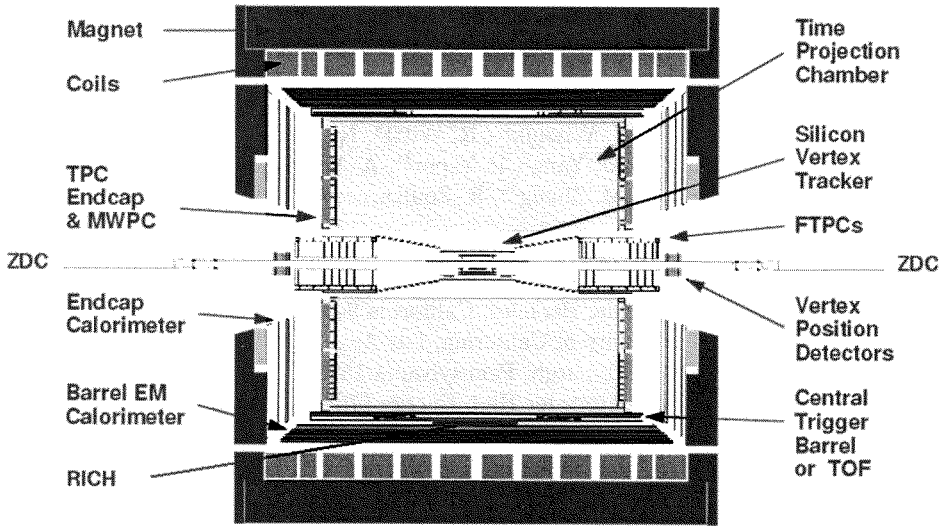

Figure 1. Side-view of the STAR experiment at RHIC.

2. The STAR Experiment

The layout of the STAR experiment [3] is shown in Fig.1. The initial configuration of STAR in 2000 consisted of a large time projection chamber (TPC) covering $|\eta| < 1.8$ and a ring imaging Cherenkov detector [6] covering $|\eta| < 0.3$ and $\Delta\phi = 20°$, inside a solenoidal magnet with 0.25 T magnetic field. The solenoid provides a uniform magnetic field of maximum strength 0.5 T for tracking, momentum analysis and particle identification via ionization energy loss measurements in the TPC. Measurements in the TPC were carried out at mid-rapidity with full azimuthal coverage ($\Delta\phi = 2\pi$) and symmetry.

2.1. Trigger

STAR utilizes a central trigger barrel (CTB) to trigger on collision centrality. The CTB, shown in Fig.1, surrounds the outer cylinder of the TPC, and triggers on the flux

of charged-particles in the $|\eta| < 1$ region. In addition, zero-degree calorimeters (ZDC) located at $\theta < 2$ mrad are used to determine the energy in neutral particles at 0 degrees [7], mostly spectator neutrons. Displayed in Fig.2 is the correlation between the summed ZDC pulse height and that of the CTB for events with a primary collision vertex successfully reconstructed from tracks in the TPC. This correlation is predominantly geometrical in origin. At large impact parameters, where the cross section is largest, only a few spectator neutrons are generated and the multiplicity in the central region is small, corresponding to low signals in both the ZDC and CTB. As the impact paramater decreases, the number of forward spectator neutrons grows rapidly, eventually saturating and then decreasing for small impact parameters. At the same time, the CTB multiplicity increases, with the most central collisions corresponding to high CTB multiplicity and a small number of forward spectator neutrons. Thus, the correlation between the ZDC and CTB can be used to provide a trigger for collision centrality.[1]

A minimum bias trigger was obtained by selecting events with a pulse height in each ZDC that was above the single neutron threshold. Triggers corresponding to smaller impact parameter were implemented by selecting events along the ZDC vs CTB curve with sufficiently large CTB signal to eliminate the second branch at low CTB values shown in Fig.2.

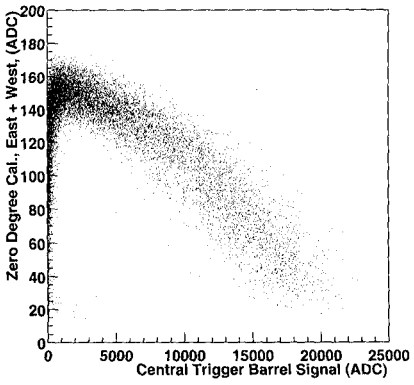

Figure 2. Correlation between pulse heights of Zero Degree Calorimeters (ZDC) and Central Trigger Barrel in a minimum bias trigger.

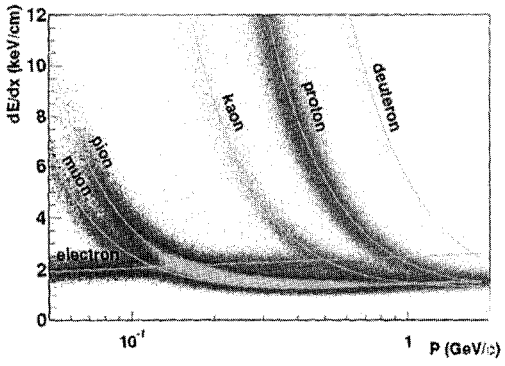

Figure 3. Ionization energy loss for charged-particles measured in the Time Projection Chamber as a function of particle momentum. Curves represent predictions of the Bethe-Bloch formula.

2.2. Detector Performance

Tracks in the STAR TPC were used to determine the distribution of the vertices of beam-beam collisions in RHIC. This was found to be 0.7 mm in the direction transverse

[1]A low signal in the ZDC may result from collisions at small or large impact parameter, as seen in Fig.2.

to the beam with a longitudinal rms length of 96 cm.[2] The standard deviation of the position resolution for track points measured in the TPC at mid-rapidity was found to be 0.5 mm. The momentum resolution was determined to be $\delta p/p < 2\%$ for tracks in the TPC with momentum p = 500 MeV/c. The ionization energy loss (dE/dx) resolution was found to reach 8 percent for tracks measured over the entire radial extension of the TPC. These performance factors are consistent with the original design specifications for the TPC in STAR [3]. For reference, the measured energy loss (dE/dx) of charged particles detected in the TPC is displayed in Fig.3. The measured dE/dx contours as a function of momentum are used in STAR to distinguish electrons, pions, kaons, protons and deuterons in the regions of particle separation in Fig.3. Predictions of the Bethe-Bloch formula are illustrated as curves on the figure. Detailed information on the TPC performance can be found in [8]. The RICH detector also performed to specifications. Details are presented in [9].

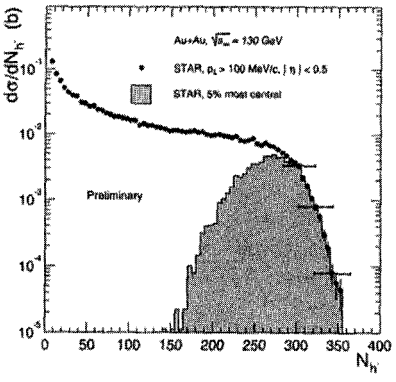

Figure 4. Multiplicity distributions of negative hadrons at mid-rapidity measured in a minimum bias trigger in STAR. See text for details.

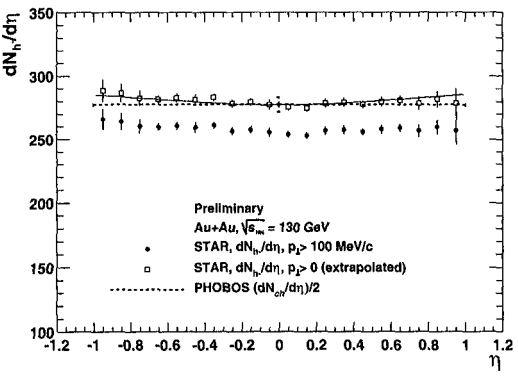

Figure 5. Pseudorapidity distributions for negative hadrons measured in STAR for the most central 5% of collisions for $p_t > 0.1$ GeV/c (solid dots) and extrapolated to $p_t = 0$ (open squares).

3. Negative Hadron Multiplicities and Spectra

Measurements of the particle multiplicity, pseudorapidity, and transverse momentum distributions provide important information on the kinetic freeze-out stage of the reaction process. This can be used to constrain theoretical descriptions of the evolution of the system from the initial hot, dense phase of the collision through chemical freeze-out

[2]This is expected to decrease by a factor of 4 in the next run with the inclusion of additional RHIC collider components.

and eventual kinetic decoupling. Shown in Fig.4 are results on the multiplicity distribution of negative hadrons for collisions of Au + Au measured with a minimum bias trigger in STAR. The transverse momentum and pseudorapidity acceptance are listed in the figure. Also shown in gray is the distribution for the 5 % most central collisions, and a solid curve depicts the predictions of a HIJING calculation [10]. The shape of the minimum bias distribution is typical of the shapes measured at lower energies and results from the collision geometry.

The pseudorapidity distribution for negative hadrons measured in STAR is displayed in Fig.5 for the 5 % most central collisions. The solid dots represent the distribution for $p_t > 0.1$ GeV/c and the open squares represent the same data extrapolated for $p_t > 0$. The measured values at $\eta = 0$ are $dN(h\text{-})/d\eta = 253 \pm 1 \pm 16$ for $p_t > 0.1$ GeV/c and $dN(h\text{-})/d\eta = 275 \pm 1 \pm 18$ for $p_t > 0$. This represents a 43 % increase in the particle multiplicity as compared to the NA49 data for Pb + Pb at $\sqrt{s_{NN}} = 17.2$ GeV [13]. The dashed line in Fig.5 shows the data published by the PHOBOS Collaboration [11] for the average charged particle multiplicity measured over the range $-1.0 < \eta < 1.0$. There is good agreement between the measurements for the average multiplicities. Pseudorapidity distributions like those measured in Fig.5 should constrain some of the important ingredients used in model calculations, particularly the initial gluon distributions and possibly the evolution in the early phase of the collisions, both of which are expected to significantly influence particle production.

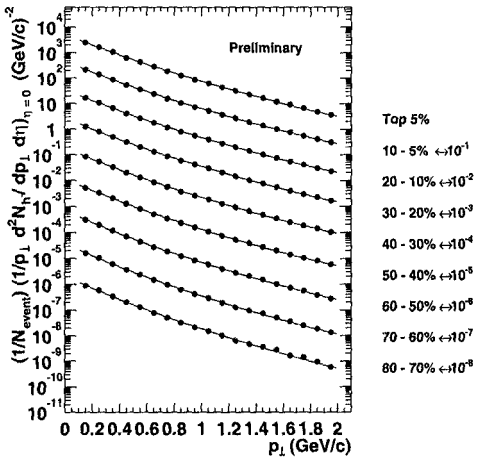

Figure 6. Preliminary transverse momentum distributions of negative hadrons measured in STAR as a function of centrality (as labeled on right side of figure).

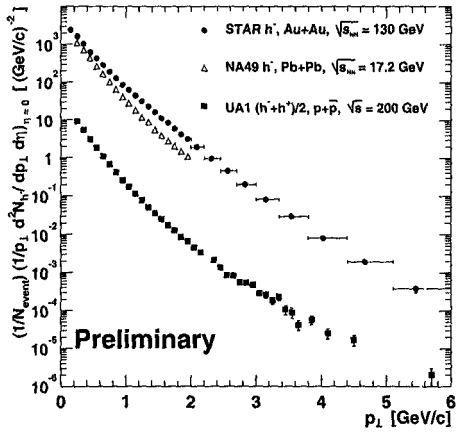

Figure 7. Transverse momentum distributions for hadrons at mid-rapidity in central Au + Au in STAR (preliminary), central Pb + Pb in NA49, and p + $\bar{p}$ in UA1.

Displayed in Fig.6 are the p_t distributions measured in STAR for negative hadrons in each of 9 centrality bins. The centrality was determined from Fig.2 with centrality

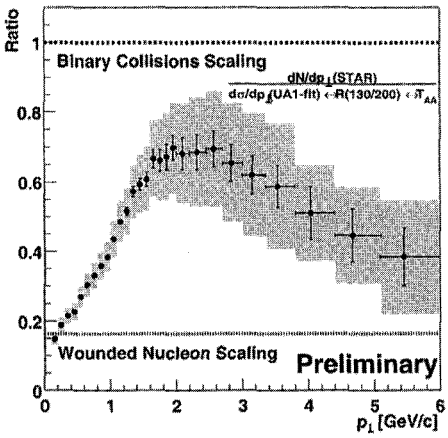

Figure 8. Ratio of the STAR negative hadron p_t distribution with the scaled UA1 average hadron p_t distribution in p + $\bar{p}$ collisions. See text for details.

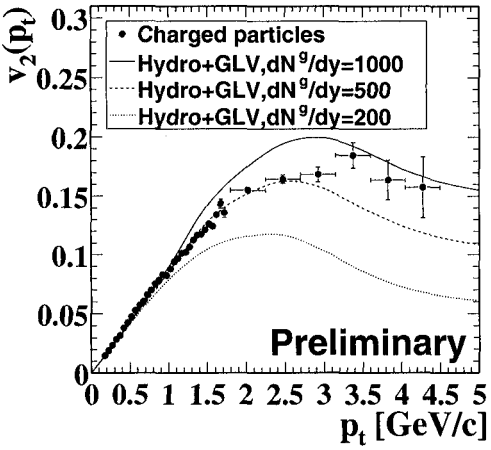

Figure 9. Data points represent the elliptic flow v_2 measured in STAR as a function of p_t. Curves represent predictions of [22].

bins corresponding to fractions of the geometrical cross section [12]. The p_t distributions follow a power law dependence as already observed at higher energies [14]. Displayed in Fig.7 is the transverse momentum distribution of negative hadrons for the most central bin of Fig.6 extended to p_t = 6 GeV/c. For comparison, the data from central collisions of Pb + Pb measured at mid-rapidity in NA49 at $\sqrt{s_{NN}}$ = 17 GeV are also displayed in Fig.7 [13], along with the transverse momentum distributions for the average of the negative plus positive hadrons in anti-proton + proton collisions measured in UA1 at $\sqrt{s}$ = 200 GeV [14]. All three distributions follow a simple power-law formulation and, as seen in the figure, the spectrum from STAR is flatter than the other two distributions. The mean p_t, deduced from Fig.6, rises slightly with decreasing impact parameter to a value of 0.514 ± 0.012 GeV/c for the most central bin in STAR. This is to be compared to a value measured in NA49 of 0.414 ± 0.004 GeV/c and in UA1 of 0.392 ± 0.003 GeV/c.

A comparison of the negative hadron p_t distributions from central collisions in STAR with those of the average hadron p_t distributions from UA1, scaled for the energy difference [16], is presented as a function of p_t in Fig.8. The ratio is normalized to have the value of unity if particle production scales as the number of nucleon-nucleon binary collisions, taking into account the nuclear geometry. The ratio at low p_t is indicative of wounded nucleon (participant number) scaling, and rises as p_t increases. It reaches a maximum near p_t = 2 GeV/c and decreases above that, signifying a suppression of the hadron yield at high p_t in central Au + Au collisions relative to the p + $\bar{p}$ reference case. The binary collision scaling value corresponds to a Au + Au overlap integral of 26 mb^{-1} for the 5 % most central Au + Au collision data, or 1050 binary collisions. The divergence

in this ratio away from the binary scattering limit suggests the exciting possibility that fragmentation products of the hard-scattered partons are suppressed in the Au + Au case due to partonic energy loss [15]. A more detailed description of this comparison is contained in ref [16].

4. STAR Elliptic Flow Measurements

STAR's inherent geometrical symmetry has allowed an early determination of the elliptic flow in collisions at RHIC [17]. Elliptic flow is the second harmonic Fourier coefficient of the azimuthal particle distribution represented by $v_2 = \langle (p_x^2 - p_y^2)/(p_x^2 + p_y^2) \rangle$, where the x and y directions are transverse to the colliding beams. Of particular interest is the large value of v_2 measured at RHIC, relative to lower values at the AGS and at the SPS. The peak elliptic flow measured at this RHIC energy in STAR reaches 6 %, while the values measured at the AGS and SPS are 2 % [18] and 3.5 % [19], respectively. Except for the most peripheral collisions, hydrodynamic calculations of v_2 agree with the STAR data. Since hydrodynamics assumes local equilibration [20], this agreement indicates that thermalization is attained early in these collisions.

New STAR measurements of the p_t dependence of the elliptic flow are presented in Fig.9. At low p_t the elliptic flow increases with p_t as predicted by hydrodynamics [20]. At high p_t where perturbative QCD is applicable, elliptic flow is expected to vanish unless there is parton energy loss in the medium to create the azimuthal asymmetry [21]. The STAR results in Fig.9 follow the hydrodynamic behavior at low p_t and level off between 2 and 4 GeV/c. The observed behavior is consistent with a model [22] incorporating hydrodynamic behavior at low p_t, and pQCD and parton energy loss in a dense medium at high p_t. The curves in Fig.9 represent different gluon densities in the calculation [22]. The similarity of the trends in Fig.8 and Fig.9 are intriguing, but not yet understood quantitatively. For more details on STAR flow measurements, see [23].

5. Identified Particle Spectra

Using ionization energy loss as displayed in Fig.3, the spectra of identified particles can be measured. Displayed in Fig.10 and Fig.11 are preliminary spectra of negative kaons and anti-protons, respectively, at mid-rapidity as a function of transverse mass (minus the rest mass) for 5 centrality bins. The anti-proton spectra were corrected for feed-down from decays using the HIJING model [10]. This correction, of the order of 20 %, is approximately constant as a function of p_t. The spectra are exponential over the transverse mass range measured. The anti-proton slopes increase with centrality from ~200 MeV for peripheral collisions to 555 ± 16 ± 50 MeV for the most central 6 % bin. A comparison of the most central 6 % centrality bins for identified π^-, K^-, and $\bar{p}$ is displayed in Fig.12. The inverse slopes of these spectra increase significantly with particle mass as shown in Fig.13 via comparison with the inverse slopes measured in NA44 [24] and NA49 [13] at CERN. This suggests a significantly increased transverse flow at RHIC as compared to the CERN SPS.

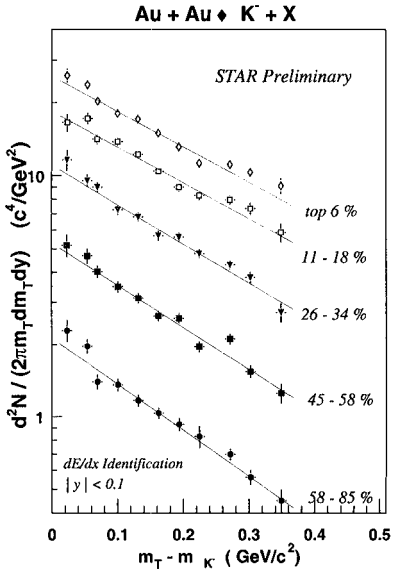

Figure 10. Transverse mass spectra for K^- at mid-rapidity in central Au + Au collisions.

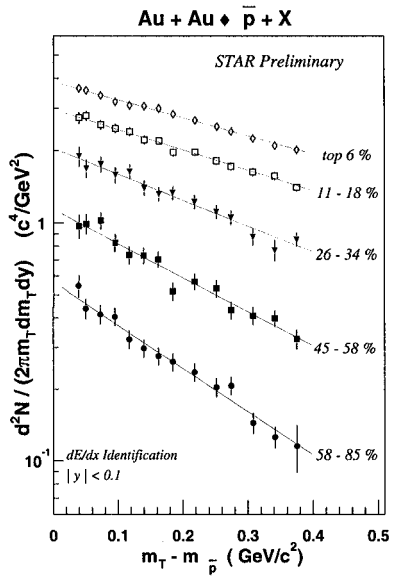

Figure 11. Transverse mass spectra for $\bar{p}$ at mid-rapidity in central Au + Au.

6. Strange Particles

To gain access to the high density phase and information on its strangeness content, strange mesons (K^+, K^-, K^o, K^{*o}, $\bar{K}^{*o}$, ϕ) and baryons ($\bar{\Lambda}, \Lambda, \Xi^-, \bar{\Xi}^+$, $\Omega^-, \bar{\Omega}^+$) can be measured in STAR at mid-rapidity [25,26]. An enhancement in the production of strange particles resulting from an equilibrated system of quarks and gluons was one of the first predictions for a signature of QGP formation [27]. Determination of the efficiencies for detecting and reconstructing these secondary decay vertices in STAR is presently underway. Preliminary results are reported in [26]. An enhancement in the strange antibaryon content [28,29] and an increased enhancement of multiply-strange baryons ($\Xi^-, \bar{\Xi}^+$, Ω) compared to singly-strange hadrons [28] have been predicted to signify the presence of a QGP. These measurements will be made with high precision in the next RHIC run, once the Silicon Vertex Tracker is installed in STAR.

7. Particle Ratios

The ratio of the yields of baryons to anti-baryons is related to baryon transport in the collision process. The measurement in STAR requires corrections, concentrated at low p_t, for secondary interactions in material which generate protons and absorb antiprotons. The anti-baryon to baryon ratios measured at mid-rapidity as a function of $\sqrt{s_{NN}}$ is shown in Fig.14 for central collision data from the AGS [31], SPS [32] and data from STAR [30,33] at RHIC. The anti-baryon to baryon ratio increases by over two orders of magnitude from the AGS to the SPS, and by another order of magnitude to the preliminary values measured in STAR. This strong increase as a function of $\sqrt{s_{NN}}$ reflects an increase in

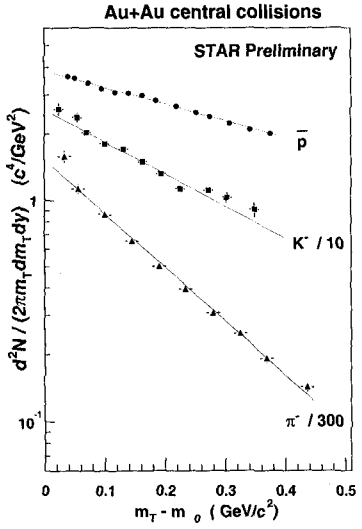

Figure 12. Transverse mass spectra for π^-, K^- and $\bar{p}$ at mid-rapidity in the 6% most central Au + Au collisions.

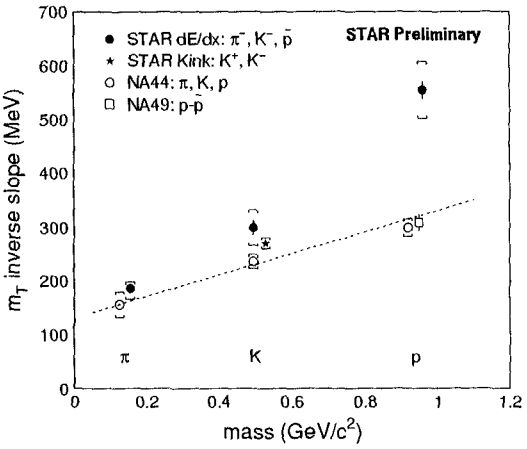

Figure 13. Inverse slope T as a function of identified particle mass in central Au + Au in STAR at RHIC and central Pb + Pb in NA44 and NA49 at CERN. Error brackets correspond to root-mean-square statistical plus systematic errors.

the baryon - anti-baryon production at higher energies. The ratio approaches, but is still slightly less than, unity which suggests that there is a slight positive net baryon density at mid-rapidity at this RHIC energy. See [33] for more details.

Fig.15 shows the ratios of various particle species measured by STAR and by SPS experiments. Comparison indicates the degree of equilibration achieved in RHIC collisions. The anti-baryon/baryon and K^-/K^+ ratios measured by STAR are consistent with a simple quark coalescence mechanism for particle formation [34].

8. Two-Pion Correlations from STAR

Correlations between identical bosons provide information on the freezeout geometry, the expansion dynamics and possibly the existence of a QGP [35]. The dependence of the pion-emitting source parameters on the transverse momentum components of the particle pairs can be measured with high statistics in STAR. In the present study a multi-dimensional analysis for identified charged pions is made using the standard Pratt-Bertsch decomposition [35,36] into outward, sideward, and longitudinal momentum differences and radius parameters. The data are analyzed in the longitudinally co-moving source frame, in which the total longitudinal momentum of the pair (collinear with the colliding beams) is zero. As expected, larger sizes of the pion-emitting source are found for the more central

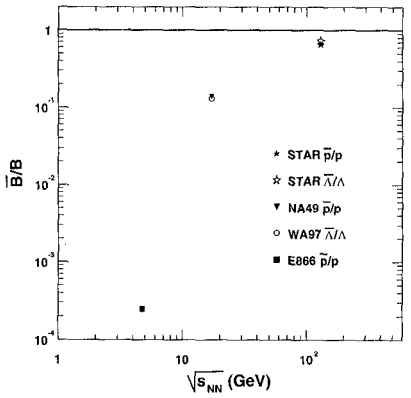

Figure 14. The mid-rapidity anti-baryon to baryon ratio as a function of $\sqrt{s_{NN}}$ from central collisions.

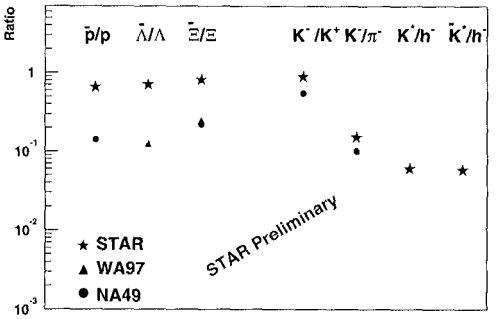

Figure 15. Various ratios of particles measured at the SPS and in STAR at RHIC.

(i.e. decreasing impact parameter) events, which have higher pion multiplicities. This source size is observed to decrease with increasing transverse momentum of the pion pair [37]. This dependence is similar to what has been observed at lower energies and is an effect of collective transverse flow. Shown in Fig.16 are preliminary results from STAR for the coherence parameter λ and the radius parameters R_{out}, R_{side}, and R_{long} extracted in the analysis. Also shown are values of these parameters extracted from similar analyses at lower energies. All analyses are for low transverse momentum ($\sim$ 170 MeV/c) negative pion pairs at midrapidity for central collisions of heavy nuclei. From Fig.16 the values of λ, R_{out}, R_{side}, and R_{long} extend smoothly from the dependence at lower energies and show no significant changes in the source from those observed at the CERN SPS energy. The anomalously large source sizes or source lifetimes predicted for a long-lived mixed phase [38] have not been observed in this study. For more details, see [37].

9. Ultraperipheral Collisions

The STAR physics program also includes the study of interactions between the two highly-charged, relativistic heavy ions at impact parameters larger than the sum of the nuclear radii. In these interactions the two nuclei act as sources of fields which interact over long range, corresponding to collisions between two photons or a photon and a pomeron. The cross sections for such collisions are large [4]. A resultant vector meson is observed by STAR through its decay into charged secondaries. Background events, which include cosmic-ray, beam-gas, nuclear, and incoherent photonuclear interactions, were suppressed by selecting events with only two oppositely-charged tracks, whose energy-loss in the TPC was consistent with pions. The transverse momentum distribution of $\pi^+\pi^-$ pairs peaks at $p_t < 100$ MeV/c, as seen in Fig.17 (top). This is consistent with coherent production from both nuclei. The invariant mass spectrum of $\pi\pi$ pairs with $p_t < 100$ MeV/c is displayed

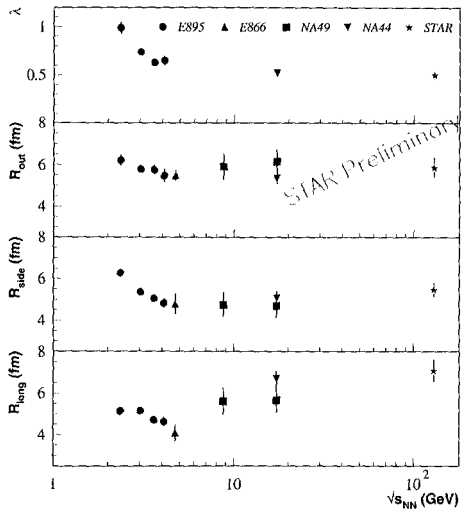

Figure 16. Measurements of the coherence parameter λ and radius parameters R_{out}, R_{side}, and $R_{longitudinal}$ from central collisions of Au + Au at the BNL-AGS, Pb + Pb at the CERN-SPS and Au + Au data from STAR.

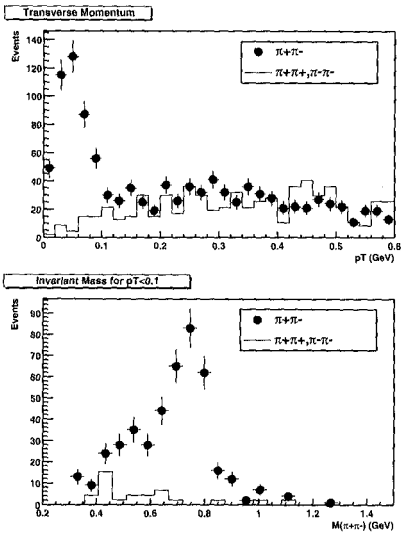

Figure 17. The p_t (top) and invariant mass (bottom) spectra of $\pi^+\pi^-$ pairs (solid points) and like-sign $\pi\pi$ pair background (histogram) with $p_t < 100$ MeV/c for two-track events.

in Fig.17 (bottom), and is observed to peak around the mass of the ρ. The like-sign pion pairs, the histogram in Fig.17, are concentrated at lower mass. This measurement of $\pi^+\pi^-$ pairs is the first observation of coherent ρ production in ultra-peripheral collisions of relativistic heavy ions. More detailed studies with higher statistics, including production of higher mass vector mesons, are expected in the next RHIC run.

10. STAR in the Next RHIC Run

Additional detectors will be added for the run in 2001. These are a silicon vertex tracker (SVT) covering $|\eta| < 1$, and a forward radial-drift TPC (FTPC) covering $2.5 < |\eta| < 4$. For the next run the barrel electromagnetic calorimeter (EMC) will reach approximately 20% of its eventual $-1 < \eta < 1$ and $\Delta\phi = 2\pi$ coverage and will allow measurement of the transverse energy of events, and trigger on and measure high transverse momentum photons and π^o's. The remainder of the EMC plus one endcap will be constructed and installed over the next 2 - 3 years. A time-of-flight (TOF) patch covering $0 < \eta < 1$ and $\Delta\phi = 0.04\pi$ will also be installed for 2001 operation to extend the particle identification for single particle spectra at midrapidity in STAR.

11. Conclusions

The STAR detector performed well during the first RHIC run. As a result, STAR has been able to make significant progress in mapping out the soft physics regime at RHIC. The anti-particle production increases relative to the SPS, and the net baryon density at mid-rapidity is lower at RHIC. The particle production is large as exhibited by a 43 % increase in charged particle multiplicity relative to measurements with heavy ions at the SPS. The negative hadron transverse momentum distributions exhibit a power-law dependence and are observed to be flatter than their counterparts at the CERN SPS and in proton + anti-proton collisions at slightly higher energy. Midrapidity spectral slopes increase with centrality and particle mass exhibiting strong transverse flow. The measured particle ratios are found to be consistent with quark coalescence. Two-particle correlation measurements exhibit source sizes similar to those measured at the CERN SPS with heavy ions. The elliptic flow measured in STAR is larger than observed at lower energies, and is in agreement with calculations using hydrodynamics. This suggests thermalization at an early stage of the collision. This strong elliptic flow is observed out to high p_t ($\sim$ 4.5 GeV/c). The high p_t negative hadron yields are suppressed in the range $2 < p_t < 6$ GeV/c relative to those in elementary collisions, suggesting large differences in parton fragmentation and/or propagation between the heavy ion and elementary cases.

Acknowledgements

We thank the RHIC Operations Group at Brookhaven National Laboratory for their support and for providing collisions for the experiment. This work was supported by the Division of Nuclear Physics and the Division of High Energy Physics of the Office of Science of the U.S. Department of Energy, the U.S. National Science Foundation, the Bundesministerium fuer Bildung und Forschung of Germany, the Insitut National de la Physique Nucleaire et de la Physique des Particules of France, the United Kingdom Engineering and Physical Sciences Research Council, and the Russian Ministry of Science and Technology.

REFERENCES

1. F. Karsch, Proceedings of this Conference.
2. see Nucl. Phys. A661 (1999) and references therein.
3. Conceptual Design Report for the Solenoidal Tracker At RHIC, The STAR Collaboration, PUB-5347 (1992); J.W. Harris et al, Nucl. Phys. A 566, 277c (1994).
4. J. Nystrand and S. Klein, nucl-ex/9811007; S. Klein and J. Nystrand, Phys. Rev. C60 (1999) 14903.
5. Proposal on Spin Physics Using the RHIC Polarized Collider, RHIC Spin Collaboration (1992).
6. A Ring Imaging Cherenkov Detector for STAR, STARnote 349, STAR/ALICE RICH Collaboration (1998); ALICE Collaboration, Technical Design and Report, Detector for High Momentum PID, CERN/LHCC 98-19.
7. C. Adler, et al. pre-print nucl-ex/0008005 (2000).
8. F. Retiere (STAR Collaboration), Proceedings of this Conference.

9. B. Lasiuk (STAR Collaboration), Proceedings of the Conference.
10. X. N. Wang and M. Gyulassy, Phys. Rev. D44 (1991) 3501; Comput. Phys. Commun. 83 (1994) 307; and private communication.
11. B.B. Back et al., Phys. Rev. Lett. 85 (2000) 3100.
12. M. Calderon (STAR Collaboration), Proceedings of the Conference.
13. H. Appelshäuser et al (NA49 Collaboration), Phys. Rev. Lett. 82 (1999) 2471.
14. C. Albajar et al., Nucl. Phys. B355 (1990) 261.
15. M. Gyulassy and M. Pluemmer, Phys. Lett. B243 (1990) 432; X.N. Wang and M. Gyulassy, Phys. Rev. Lett. 68 (1992) 1480.
16. J.C. Dunlop (STAR Collaboration), Proceedings of the Conference.
17. K.H, Ackermann et al (STAR Collaboration), Phys. Rev. Lett. 86 (2001) 402.
18. J. Barrette et al (E877 Collaboration), Phys. Rev. C55 (1997) 1420.
19. A.M. Poskanzer and S.A. Voloshin (NA49 Collaboration), Nucl. Phys. A661 (1999) 341c.
20. P.F. Kolb, J. Sollfrank, and U. Heinz, pre-print hep-ph/0006129 v2 (2000).
21. X.N. Wang, preprint nucl-th/0009019 (2000).
22. M. Gyulassy, I. Vitev, and X.N. Wang, preprint nucl-th/0012092 (2000).
23. R. Snellings (STAR Collaboration), Proceedings of this Conference.
24. I.G. Bearden et al. (NA44 Collaboration), Phys. Rev. Lett. 78 (1997) 2080.
25. Z. Xu (STAR Collaboration), Proceedings of this Conference.
26. H. Caines (STAR Collaboration), Proceedings of this Conference.
27. J. Rafelski and B. Müller, Phys. Rev. Lett. 48 (1982) 1066. [Erratum: *ibid.* 56 (1986) 2334.]
28. J. Rafelski, Phys. Rep. 88 (1982) 331.
29. P. Koch, B. Müller and J. Rafelski, Phys. Rep. 142 (1986) 167 .
30. C. Adler et al. (STAR Collaboration) Phys. Rev. Lett. (2001) in press.
31. L. Ahle et al (E802 Collaboration), Phys. Rev. Lett. 81 (1998) 2650.
32. F. Sikler et al (NA49 Collaboration), Nucl. Phys. A661 (1999) 45c.
33. H. Huang (STAR Collaboration), Proceedings of this Conference.
34. J. Zimanyi, et al., preprint (2001) to be published in World Scientific.
35. S. Pratt, Phys. Rev. D33 (1986) 1314; G. Bertsch, M. Gong and M. Tohyama, Phys. Rev. C37 (1988) 1896; and G. Bertsch, Nucl. Phys. A498 (1989) 151c.
36. S. Pratt et al., Phys. Rev. C42 (1990) 2646.
37. F. Laue (STAR Collaboration), Proceedings of this Conference.
38. D. H. Rischke, Nucl. Phys. A610 (1996) 88c; D.H. Rischke and M. Gyulassy, Nucl. Phys. A608 (1996) 479.